REPORT DOCUMENTATION PAGE

Form Approved
OMB No. 0704-0188

1. REPORT DATE *(DD-MM-YYYY)*	2. REPORT TYPE	3. DATES COVERED *(From - To)*
	Final	08/01/10 - 12/31/11

4. TITLE AND SUBTITLE

Pliant Micro Membrane-Wing Tip Vorticity Estimation Using Strain Sensitive Active Materials

5a. CONTRACT NUMBER

5b. GRANT NUMBER
FA9550-10-1-0325

5c. PROGRAM ELEMENT NUMBER

6. AUTHOR(S)

R Albertani

5d. PROJECT NUMBER

5e. TASK NUMBER

5f. WORK UNIT NUMBER

7. PERFORMING ORGANIZATION NAME(S) AND ADDRESS(ES)

University of Florida
Gainesville FL 32611
Oregon State University
Corvallis Oregon 97331

8. PERFORMING ORGANIZATION REPORT NUMBER

9. SPONSORING / MONITORING AGENCY NAME(S) AND ADDRESS(ES)

AF Office of Scientific Research
875 N Randolph St
Arlington VA 22203

10. SPONSOR/MONITOR'S ACRONYM(S)

11. SPONSOR/MONITOR'S REPORT NUMBER(S)

12. DISTRIBUTION / AVAILABILITY STATEMENT

13. SUPPLEMENTARY NOTES

14. ABSTRACT

A mathematical correlation between wing-membrane discrete strains, wing lift and tip vorticity intensity, with simplified assumptions, was formulated and demonstrated.
Wing circulation and lift estimation from tip vorticity, obtained via PIV measurements correlated qualitatively well with sting balance data from wind tunnel tests.
The elastic pliant wing membrane shape under aerodynamic loads was estimated using a discrete number of strain information simulating patches of strain sensitive sensors on the surface of the wing. The information provided from the simulated stain sensors was used to reconstruct a quadratic representation of actual deformed membrane surface. A linear partial differential equation relating pressure distribution to membrane deflection is used to relate and correlate wing structural strain to lift and wing-tip vorticity via approximating lift resultant and applying basic linear aerodynamic principles.
The models can account for the pliant wing membrane different levels of pre-tension. Using relatively simple, low order approximations, a distinct correlation between strain, wing-tip vorticity and lift has been presented and demonstrated.
An investigation of the trade-off of more complex flow and pressure state solver options versus simple aerodynamic principles should be investigated in the future.

15. SUBJECT TERMS

Mathematical correlation between wing-membrane strains, wing lift and tip vorticity, wing membrane shape estimated using a discrete patches of strain sensitive sensors on the surface of the wing.

16. SECURITY CLASSIFICATION OF:			17. LIMITATION OF ABSTRACT	18. NUMBER OF PAGES	19a. NAME OF RESPONSIBLE PERSON
a. REPORT	b. ABSTRACT	c. THIS PAGE	SAR	24	Roberto Albertani
	U				19b. TELEPHONE NUMBER *(include area code)* 541-737-7024

Standard Form 298 (Rev. 8-98)
Prescribed by ANSI Std. Z39.18

Final Technical Report

Pliant Micro Membrane-Wing Tip Vorticity Estimation using Strain Sensitive Active Materials

Contract Number: FA9550-10-1-0325

Submitted by:

Dr. Roberto Albertani, coPI
Associate Professor
School of Mechanical, Industrial and Manufacturing Engineering
Oregon State University, Corvallis, OR
Email: Roberto.Albertani@oregonstate.edu

Submitted to:

Dr. Douglas R. Smith Civ USAF AFMC AFOSR/RSA
Flow Interactions & Control, Program Manager
Air Force Office of Scientific Research
875 N Randolph St, Suite 325, Room 3112
Arlington, VA 22203
ph: 703.696.6219
email: douglas.smith@afosr.af.mil

February, 2012.
Total number of pages: 24.

Project summary.

The goals planned for this project have been achieved.

A mathematical correlation between wing-membrane discrete strains, wing lift and tip vorticity intensity, with simplified assumptions, was formulated and demonstrated.

Wing circulation and lift estimation from tip vorticity, obtained via PIV measurements correlated qualitatively well with sting balance data from wind tunnel tests. The experimental results and theoretical models of lift estimation from vorticity are in agreement and both underestimate the measured lift, as expected.

The reason is likely to be the fact that the tip vortex does not contain the complete lift circulation energy and will therefore never be completely capable of providing the full force estimation.

The elastic pliant wing membrane shape under aerodynamic loads was estimated using a discrete number of strain information simulating patches of strain sensitive sensors on the surface of the wing. The information provided from the simulated stain sensors was used to reconstruct a quadratic representation of actual deformed membrane surface. A linear partial differential equation relating pressure distribution to membrane deflection is used to relate and correlate wing structural strain to lift and wing-tip vorticity via approximating lift resultant and applying basic linear aerodynamic principles. The models can account for the pliant wing membrane different levels of pre-tension. This estimation has been developed with a low order approximation of the shape the wing-membrane assumes and of the dynamic pressure applied to it. With higher order models it is likely that the absolute accuracy of these estimations could be improved.

Nevertheless, even with simple, low order approximations, a distinct correlation between strain, wing-tip vorticity and lift has been presented and demonstrated.

An investigation of the trade-off of more complex flow and pressure state solver options versus simple aerodynamic principles should be investigated in the future. Perhaps coupling of a panel solver to a finite element membrane model with strain estimation could yield an algorithm which uses both aerodynamic and structural theory to minimize the estimate error of both load and structural deformation in an iterative fashion.

Publications

• Albertani, R., Ray, C., "Tip Vorticity and Membrane-Strain Analysis on a MAV Elliptical Pliant Membrane-Wing," Presented at the *6th AIAA Theoretical Fluid Mechanics Conference*, Fluid Mechanics of Micro Air Vehicles Invited Session, Honolulu, Hawaii, June 27-30, 2011.

• Carpenter, T., Ray, C., Albertani, R., "Correlation of Structural Strain to Tip Vorticity and Lift for a MAV Pliant Membrane Wing," accepted for presentation at the *SEM XII International Congress & Exposition on Experimental and Applied Mechanics*, Costa Mesa, CA, June 11-14, 2012.

EXCERPT FROM FIRST PHASE.

Wing design.
The experimental activities were carried out with several wings having identical basic elliptical planform shape with a wingspan of 0.200 m, an aspect ratio of two, an area of 0.0157m^2, and a mean aerodynamic chord of 0.0849 m. A rigid wing, made by solid aluminum thin plate bonded on a slightly thicker steel perimeter, was used as a reference for the aerodynamic coefficients and wing-tip vortex structure. Wings with identical planform dimensions and rigid perimeters are used with the pliant elastic latex membrane attached to the perimeter. The elastic membranes are set with different levels of pre-strain. The thickness and density of the latex membrane is estimated 0.1016±0.0508 mm and 980 kg/m^3. The average measured thickness of the membrane is 0.15±0.01 mm.

Experimental set up: wind tunnel.
The experiments were carried out at the low-speed open-loop, open-jet wind tunnel at the University of Florida's Research, Engineering and Education Facility (REEF). The test section, one by one meter with an axial length of three meters, is surrounded by a structural enclosure. A typical installation of the MAV wing in the wind tunnel is illustrated in Fig. 1. The particle image velocimetry (PIV) system used during the initial tip velocities characterization on the rigid wing is a three-dimensional LA Vision system with stereo-vision cameras, as illustrated in Fig. 2. Olive oil was used for seeding.

Figure 1. Installation of the wing in the wind tunnel. The model is mounted on the sting balance.

Figure 2. Installation of the wing in the wind tunnel. The PIV cameras are visible in the background.

General and Theoretical Methodology.
Wind tunnel experiments were performed to investigate the aerodynamics and pliant wing membrane elastic deformation on an elliptical wing of typical MAV dimensions. The objective of the aerodynamic part of this work was to correlate the wing-tip vortex field with the wing lift data obtained using a sting balance. A PIV was used for wing-tip vortex measurements while visual image correlation (VIC) system was used to quantify the membrane wing strain state.

Results.
In the first phase of this research, two objectives have been successfully carried out: 1) MAV rigid-wing tip vorticity characterization, with the estimate of lift, and 2) wing-membrane strain state measurements.
The vortex snapshot PIV data was used to estimate the coefficient of lift for the wing and compared with the result obtained by the sting balance measurements. Estimated values for lift coefficient agree with those measured by the sting balance and behave as expected for varying AOA. The results for the lift theoretical calculation from circulation and associated variation (± one standard deviation) with the sting balance values are illustrated in Fig. 3.

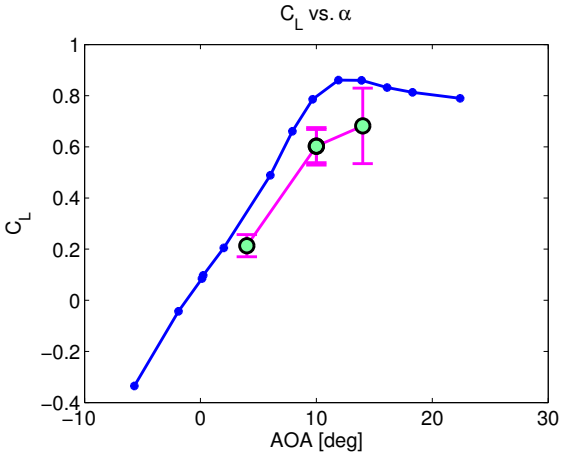

Figure 3. Comparison of coefficient of lift (C_L) vs angle of attack for sting balance data (blue) and vortex date estimates. Four data points are plotted. Two estimates for coefficient of lift, calculated at different free-stream velocities, are collocated.

A comparison of coefficient of lift vs. angle of attack for the rigid and membrane wings is illustrated in Fig. 4. Note how the lift coefficient for the membrane wing continues to increase well after the rigid wing stall angle of approximately 10 degrees. This is due to the adaptive camber effects of the flexible membrane, well documented in the author's previous work.

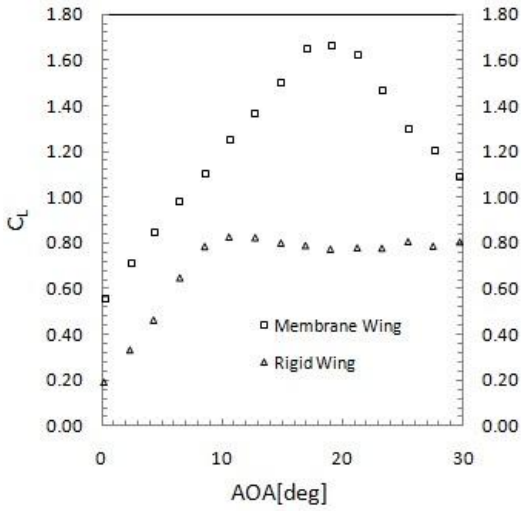

Figure 4. Comparison of CL vs. AOA as collected by sting balance for rigid wing and membrane wing used in experiment.

A sample of the strain state in the two body-frame directions X and Y are illustrated in Fig. 5 and 6, respectively. The airflow direction is left to right. Experimental conditions are 10 m/s at an angle-of-attack of 15 degrees. The average membrane strain in the chordwise direction is one order of magnitude larger than the spanwise direction. The average strain level in X direction is approximately 10,206 μstrain, whereas in the Y direction is approximately 1,790.5 μstrain. Negative strain observed in the Y direction at the trailing edge, as illustrated in Fig. 6. It was due to a creep phenomenon within the bonding of the pre-stressed latex to the carbon fiber. Therefore the results show the relaxation of the pre-stretched membrane.

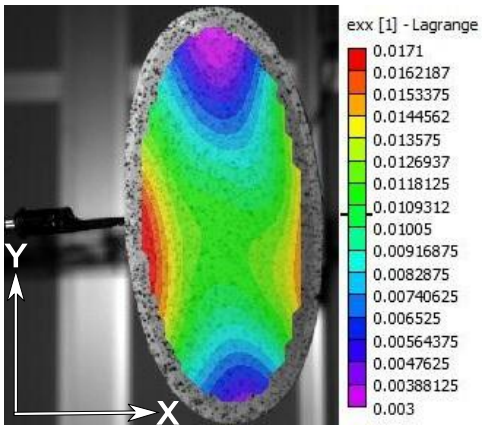

Figure 5. Strain-state ε_{xx} on the wing-membrane during a run in the wind tunnel at 10 m/s and 15^0 angle-of-attack. Flow is from right to the left. Pockets of low strain are noticeable in the wing tips areas.

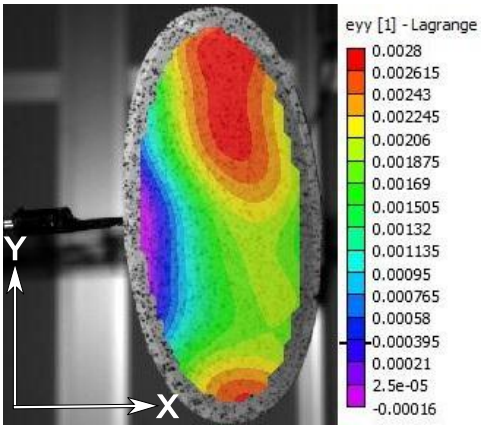

Figure 6. Strain-state ε_{yy} on the wing-membrane during a run in the wind tunnel at 10 m/s and 15^0 angle-of-attack. Flow is from right to the left. A pocket of low strain is noticeable in the wing trail- ing edge area.

SECOND PHASE

Experimental Setup

During testing our objective was to determine the out-of-plane deformation of the membrane wing under steady aerodynamic loads, in different steady conditions of angle of attack (AOA) and free stream velocity. The low-speed wind tunnel at Oregon State University was used to conduct this phase of testing and can be seen in Figure 7. The close loop, close test section wind tunnel is capable of speeds from 1 – 18 m/s and has a 1.3 x 1.5 meter test section. The installation of the test wing is shown in Figure 8 attached to a one degree of freedom motion rig. The apparatus was used for AOA sweeps in steady state conditions. The angle of the apparatus was measured by an inclinometer sensor with a accuracy of 0.1 degrees. Loads were measured using a six degree of freedom strain gauge load cell. The load cell was capable of measuring loads up to 100N normal force and 200N axial force with a resolution of 0.05N and 0.10N respectively. The wind tunnel flow velocity was monitored by a pitot tube probe installed in the test section ahead of the model connected to a pressure transducer with a resolution of 0.05 mmH20. Air temperature was monitored by a J-type thermocouple sensor mounted inside the test section. All channels were monitored simultaneously and recorded during testing.

For this test, the three main testing variables considered were membrane pre-strain (PS), wing AOA and wind velocity (V). To design the experiment to yield results which would be readily relatable to one another, with regard to pre-strain (i.e. deflection ranges were not on completely different scales from one another); PI2 values, as defined by [1], were considered with respect to their velocity. Π_2 is defined as,

$$\Pi_2 = \frac{\varepsilon_{ps} \times}{q \times}$$

where εps is the membrane pre-strain, t is the membrane thickness, q the dynamic pressure applied to the membrane, and c the wing chord length.

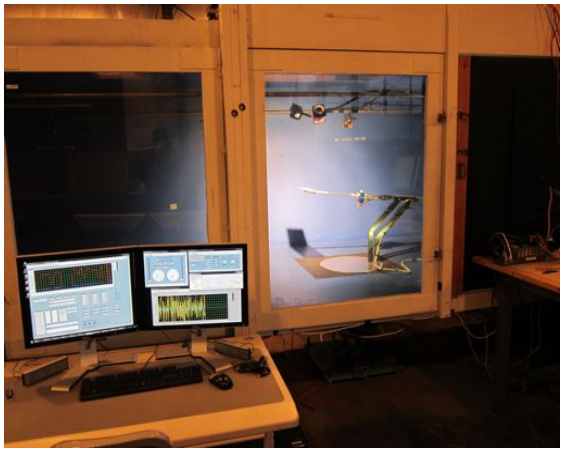

Figure 7. Exterior view of the test section of the low speed closed loop, closed test section wind tunnel at Oregon State University.

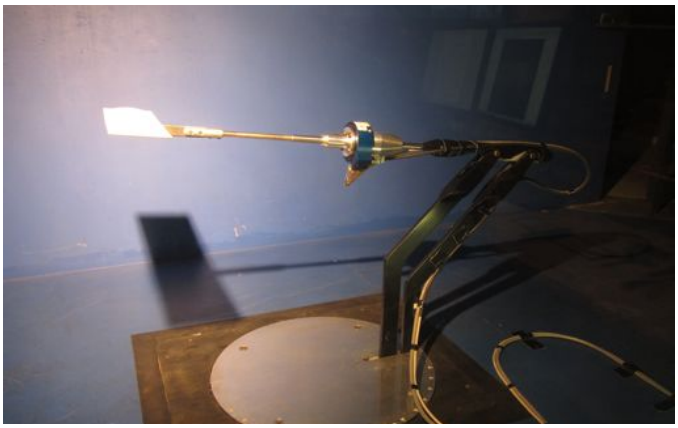

Figure 8. Membrane wing with test fixture, inside the wind tunnel.

Using a velocity range known to be relevant to MAV's yielding Re between 60000 and 90000, values of pre-strain were chosen such that the max value of PI2 for a given membrane would span the minimum range of the next membrane PS. The values of PI2 chosen for the test can be seen in Figure 9.

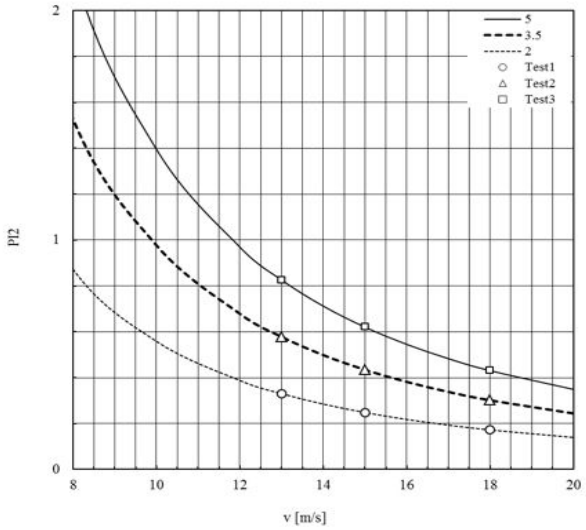

Figure 9. PI2 values versus velocity; data points chosen for wind tunnel testing and values of membrane PS chosen.

Values for AOA were chosen such that the wing would not experience flow separation, i.e. remain in the linear region lift (example can be seen in Figure 7), thus resulting in predicable behavior easily characterized by linear aerodynamic theory. From preliminary testing results, a linear lift behavior was observed between AOA of 0-10 degrees for membrane's with 2% and 5% pre-strain, given the intended panform discussed below. Due to interest in tip vorticity, it was also desired to have sufficiently high AOA such that strong predictable vortices were generated. From these requirements an AOA range of 3-9 degrees was chosen. In order to limit the number of data sets taken to a reasonable amount, three values were chosen for each of the three variables. This yielded a factorial design space of 33 or 27 tests. The resulting test matrix can be seen in Table 1.

Table 1. Test Matrix

Wind Tunnel Test Matrix		
PS [%]	**AoA**	**V [m/s]**
2	3	12
		15
		18
	6	12
		15
		18
	9	12
		15
		18
3.5	3	12
		15
		18
	6	12
		15
		18
	9	12
		15
		18
5	3	12
		15
		18
	6	12
		15
		18
	9	12
		15
		18

For the final phase of testing a rectangular planform wing with an aspect ratio of ~4 was chosen. A rectangular domain lends itself to linear theory structurally and is well-characterized aerodynamically. Aerodynamically, it is well-known that rectangular wings generate strong wing-tip vortices (relative to other planforms); the tip vortices contain much of the wake flow energy and are highly indicative of the induced drag for a rectangular shape compared to other planforms. This allows closer comparison and correlation of strain to such aerodynamic effects, although any planform should still exhibit the same correlation due to the relationship of aerodynamic effects and structural deformation in flexible wings. An aspect ratio of 4-6 was chosen to be great enough to apply traditional aerodynamic analysis, such as lifting line theory, to the model to immediately compare measured and estimated quantities including lift

and circulation. Structurally, a rectangular membrane under sufficient pretension exhibits behavior capture by the Poisson equation on a rectangular domain. This simplifies computation greatly and allows for a convenient rectangular domain to be defined and used directly with exported VIC data. The 1mm thick rectangular frame geometry can be seen in Figure 10.

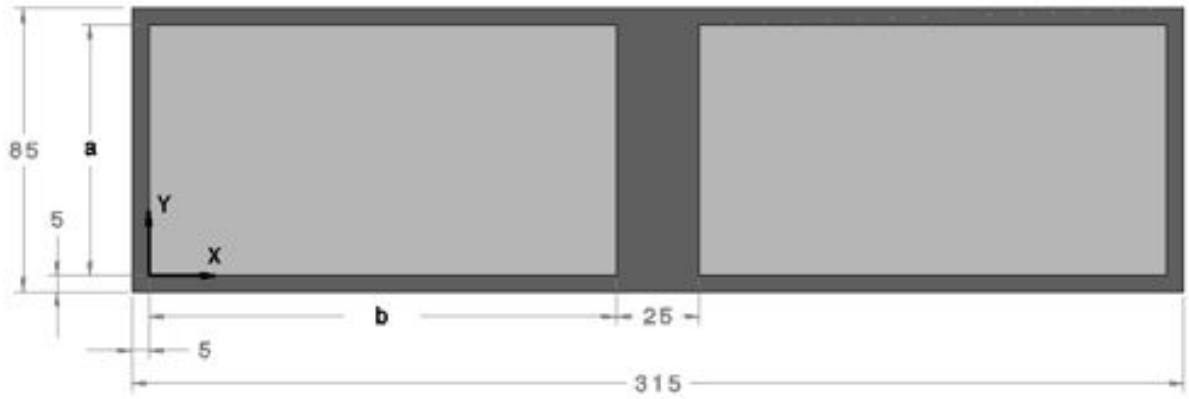

Figure 10. Schematic showing the wing frame (dark grey), the frame's dimensions and domain of the individual membrane areas (light grey).

Full-field measurements of strain and deflection of the membrane wing were performed using a visual image correlation (VIC) technique originally developed by researchers at the University of South Carolina [2, 3]. Images are captured with two high-speed AOS S-PRI cameras, capable of 1000 frames per second and capable saving 1000 frames at a resolution of 1280x1024 in an in-camera flash-memory buffer. The cameras were positioned outside and above the wind tunnel and viewed through a clear window. The reference image to measure the displacement was of the wing at the specified angles of attack, with zero wind velocity. In this case, the wing was only loaded by the skin pretension applied during the fabrication. Because we used this condition to take the reference images for the VIC, the pretension will not appear in our results. This condition needs to be carefully considered in the evaluation of the results, since this can generate areas of "virtual" compression in the skin membrane, which is of course physically not possible, due to areas of relaxation of the pre-existing tension. The sequence of events for a test was first to take a picture of the model at the set angle, with wind off. Next was to set the airspeed to the desired dynamic pressure, and when stable conditions were reached, take the picture of the deformed wing. Then the wind is stopped, and the model is moved to the next AOA. At the same time, the system was recording the aerodynamic loads. This sequence was repeated for three wings with different membrane pretension for the selected angles of attack, 3, 6 and 9 degrees at the selected nominal wind velocities 18, 15, and 12 m/s. The aerodynamic characteristics and the deformations of the different wings have also been compared to a nominally rigid wing built from a plate of this aluminum, attached to the same frame.

Force Estimation from Vorticity

In this work, several objectives have been achieved using wind tunnel testing, numerical models and analytical models in order to estimate lift. Aerodynamic loads, VIC deformation and VIC strains were captured for three membrane wings of different pretensions. The surface deformation of the membrane was reconstructed to fit a quadratic basis function using pseudo strain gauge sensors from VIC data and the aerodynamic lift generated has been estimated. Using the same surface reconstruction information, a 3D solid model of the deformed membrane wing has been generated and a CFD analysis was performed. Using the wake information generated from this analysis, aerodynamic lift was estimated from the tip vorticity.

Surface Reconstruction

In this work, we assume that the Poisson equation can be used to describe the membrane-wing used in experiment, and proceed to use a simple least-squares approach to estimation of membrane deformation from strain sensors strategically placed throughout the membrane domain as described above. To be specific, we utilize strain data (from VIC post-processing) to find an average strain value over small rectangular regions, and assume furthermore, that such a strain value approximates what might be returned by a real strain sensor that lacks directionality in its measurement.

In this approach, lift is estimated by first reconstructing the out-of-plan deformation of the membrane using pseudo strain sensors and a simple analytic model. To create the strain sensor, VIC stain data was collected over the full deformed area of the wing during wind tunnel testing. The full field strain domain was then partitioned into smaller individual areas, or "patches", representing the strains which would be present on a sensor in that given location and over that given area. Using this technique, any combination of sensor quantity, size and location could be used.

Assuming the wake flow from the wing can be captured by a low order dimensional model of the surface, which has shown to be a valid assumption [4, 5, 6]; the pressure distribution applied to the membrane is assumed to be constant, resulting in a deformation which can be represented by a close form quadratic function. Using this assumption, the out-of-plan deformation of the membrane over the domain, $0 \le x \le a$ and $0 \le y \le b$, where a and b represent the dimension of the membrane boundary in the x and y direction respectively, was modeled as,

$$w(x,y) = \frac{\alpha x(x-a)y(y-b)}{a^2/4 \times b^2/4}$$

Where α is a constant which represents the max amplitude of deformation. Independently differentiating Eq 1.1 with respect to x and y, respectively yields,

$$\frac{\partial w}{\partial x} = 2\alpha(x-a)y(y-b)$$
$$\frac{\partial w}{\partial y} = 2\alpha x(x-a)(y-b)$$

For a membrane subject to an evenly distributed load with small deformations, it is assumed that in-plane deformations are negligible and thus, strains are purely a result of out-of-plane deformation. Using this assumption, directional strains can be approximated as,

$$\varepsilon_x = \frac{1}{2}\left(\frac{\partial w}{\partial x}\right)^2, \quad \varepsilon_y = \frac{1}{2}\left(\frac{\partial w}{\partial y}\right)^2$$

Using Eq. 1.1-1.3 an analytic formulation of strain over the wing domain $0 \le x \le a$ and $0 \le y \le b$, can be defined as,

$$C(x,y) = \frac{\alpha^2}{2}\left[\left(2(x-a)y(y-b)\right)^2 + \left(2x(x-a)(y-b)\right)^2\right]$$

Assuming a strain sensor is used on the membrane surface which provides a non-directional strain output and has an area of s; VIC strain data over that area can be used to represent the sensor output as,

$$\varepsilon_i = \frac{\varepsilon_{x_i} + \varepsilon_{y_i}}{2}, \text{ where}$$

$$\varepsilon_{x_i} = \frac{1}{s_i}\int_{s_i} \varepsilon_x(x,y)ds,$$

$$\varepsilon_{y_i} = \frac{1}{s_i}\int_{s_i} \varepsilon_y(x,y)ds,$$

Given n number of strain sensors, a strain sensor vector array is defined,

$$\mathbf{S} = \begin{bmatrix} \varepsilon_1 \\ \varepsilon_2 \\ \vdots \\ \varepsilon_n \end{bmatrix}$$

Using Eq 1.5 we can define a corresponding matrix to that in Eq 1.6 evaluated at the locations of each sensor. Further, observing from Eq 1.1 that α is a constant throughout the domain, it can be factored out of the matrix as a constant,

$$\mathbf{C} = \alpha^2 \begin{bmatrix} C'_1 & C'_2 & \cdots & C'_n \end{bmatrix}$$

where $C'_i = C_{ii}/\alpha^2$. Finally, by equating Eq 1.6 and 1.7, a formulation is derived which can be used to solve for α,

$$\mathbf{S} = \alpha^2 \mathbf{C} \qquad \alpha = \sqrt{\left(\mathbf{C}^T\mathbf{C}\right)^{-1}\mathbf{C}^T\mathbf{S}}$$

Given the inherent variability in the output of the strain sensors, the variability in membrane structural properties, and irregularities in the fluid flow; solving for α in this manner yields a least squared approximation of the constant α. Thus, this formulation generates a quadratic surface which best describes the actual out of plane deformation of the membrane. With this surface reconstruction, a numeric fluid simulation can be performed to determine fluid behavior in the wake of the wing.

Numeric Fluid Model

A three dimensional, steady state, computational model was used to compute the fluid behavior induced by the deformed membrane wing. For typical MAV's, Reynolds numbers (Re) based on wing chord length are commonly in the range of 10e4 to 10e5. With the given test wing described above, placed in a flow with a Re of 10e5 in air at 25 degrees Celsius and atmospheric pressure, would yield

a Mach number of 0.052, allowing an incompressible fluid assumption to be reasonably applied to the simulation. A symmetrical boundary condition was applied at the centerline of the wing model in order to reduce computation time. The half span simulation volume was sized to be five times larger than the chord in the flow direction and two chord lengths above and below the wing and one to the side of the wing. The volume was discretized into approximately 1.2 million hexahedral volume cells with a cell width of >0.1mm in the near wake region, with cells growing to 10mm near the simulation boundaries. The Reynolds Averaged Navier Stokes (RANS) equations were solved for an incompressible flow using the Spalart-Allmaras turbulence model. As shown by [7, 8] the Spalart-Allmaras turbulence model proves to perform well in near wake regions such as wing tip vortex flows while remaining relatively computationally inexpensive.

The simulation used a computer-aided-design (CAD) model of the deformed membrane and the frame to which the membrane was attached, Figure 11. The surface of the membrane was modeled to match the quadratic form from Eq. 1.1. For a particular dynamic pressure and AOA, the surface deformation constant from Eq. 1.9 was calculated and a CAD model was generated to match. A side-by-side comparison of the actual deformed membrane during wind tunnel testing and the corresponding CAD model can be seen in Figure A-1, Appendix A. It is important to note that the simulation used is steady state, time averaged, with non-moving boundaries. Due to this simplification, simulations were limited to AOA below laminar separation.

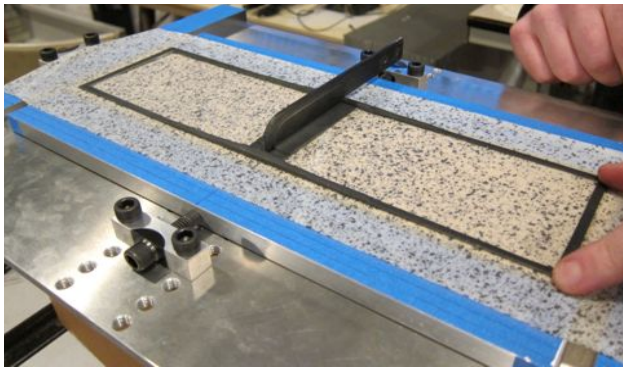

Figure 11. Speckled latex sheet attached to pre-tensioning jig with wing frame.

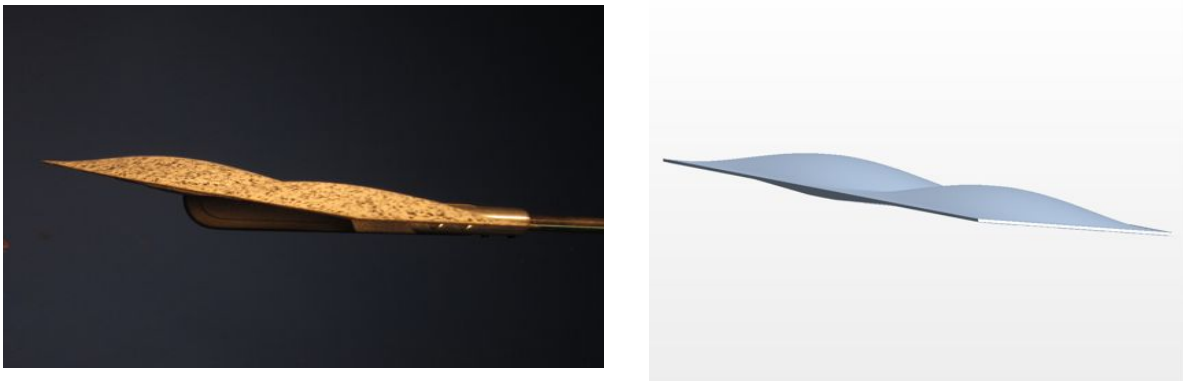

Figure 12. Speckled latex membrane wing during wind tunnel testing (left) and CAD model generated from the strain sensor surface reconstruction.

Lift from Circulation

For the purpose of this analysis, a simplified version of lifting line theory was utilized. The horseshoe vortex is a simplification of Prandtl's continuous lifting line theory. In this model, all vorticity is assumed to be present in a vortex of constant circulation bound to the wing. The bound vortex is connected at the wing-tips to two trailing vortices which extend, in theory, back to the starting vortex itself (thus forming a loop). This results in a shape reminiscent of a horseshoe in the local region of the wing, as illusyrated in Fig. A-2. For flight vehicles at the scale of MAVs, the vortices have been demonstrated to dominate the wake.

The Kutta-Joukowski theorem for steady flight states that lift is proportional to circulation as follows:

$$\frac{\partial L}{\partial y} = \rho U \, \Gamma$$

where is the lift per unit span (if y is in the spanwise direction and x the chordwise), ρ is the fluid density, U is the free stream velocity, and Γ is circulation per unit span. Circulation can be related to vorticity by Stokes' theorem:

$$\Gamma = -\oint_C V \cdot ds = -\iint_S \left(\nabla \times V\right) \cdot dS$$

where V is the flow velocity vector field, S is an area containing the vortex and C is the boundary (and a closed curve) of S. Thus, using flow information from the CFD simulation taken downstream of a wing, an estimation of the lift of the craft can be obtained by applying these basic relationships.

Force Estimation from Poisson Model

It is well documented that the linear Poisson equation, a partial differential equation, can be used to model a membrane under sufficient pretension undergoing small deformations. This section will briefly outline how by using the estimation of membrane deformation from strain, outlined above, can be used to obtain a rough estimate of the pressure distribution present on the membrane-wing -- a quantity obviously indicative of lift and strength of wing-tip vortex circulation given a specific wing geometry and linear aerodynamic theory.

The two dimensional Poisson equation is obtained through linearization of nonlinear membrane dynamical equations and/or minimization of energy of an axially deforming planar structure undergoing very small transverse displacements. Such assumptions allow rotation angles of the structure and internal tension resultants to be represented as spatial derivatives and scalar constants, respectively. Thus, such a linear model is actually a model capturing the membrane's resistance to change its internal state of stress. Such approximations, although seeming fairly crude, have nonetheless been used in the past to model membranes with success, and become increasingly accurate as pretension increases and maximum deformation decreases. The Poisson equation can be written for a rectangular domain as,

$$T_x \frac{\partial^2 w}{\partial x^2} + T_y \frac{\partial^2 w}{\partial y^2} = F(x, y)$$

where Tx and Ty are the pretension resultants in the x and y directions, respectively, and F(x, y) is the resultant pressure distribution on the membrane. Associated with this equation are boundary conditions for all edges of the domain, describing fixed edges (displacement is zero).

If one makes an assumption regarding the functional form of the deformation of the membrane, i.e. quadratic in nature, the approach here simplifies greatly. Suppose the membrane deformation can be represented by a single quadratic surface interpolating the boundaries of the membrane (thus satisfying the boundary conditions of Poisson's equation explicitly). Such a surface can be written as that used in Eq 1.1. Once α is determined from Eq 1.9, an estimate of the pressure distribution can be immediately found by simply substituting the equation for w(x, y) back into Poisson's equation using the estimated value of α. Taking second derivatives of w(x, y) and substituting into Poisson's equation yields an estimate of F provided the strain values observed on the membrane.

It should be noted that it is not expected that this approach will yield a realistic pressure distribution in general. It is an approach that, in theory, can be generalized to include more complex functional forms for displacement and/or pressure distribution. The pressure distribution itself may not be spatially accurate, but the deformation in the membrane will be and thus, the approach should approximate, at the very least, the force resultant, and therefore total lift, present on the membrane.

Estimation of circulation from strain is slightly more convoluted than reconstruction of wing surface. Classical aerodynamic theory states that the derivative of lift with respect to span is proportional to circulation, as described in Eq 1.10. Thus, one approach is to utilize the estimated force from Poisson's equation above, and simply integrate this result analytically with respect to chord. This yields an expression that describes the lift per unit span. If one were to integrate again with respect to span, the total lift resultant would be obtained. Therefore, by the fundamental theorem of calculus, one can integrate the estimated pressure distribution with respect to x to yield an expression also describing the lift per unit span. Equating this to circulation using the classical expression for circulation as given in Eq 1.10, one may simply divide by ρ*U to obtain an estimate for circulation. This provides a first-order model-based approach to estimating circulation directly from strain.

The approach described above does appeal to intuition although it is not expected to be tremendously accurate. For instance, it is well known that circulation is wing-geometry dependent, thus the fact that the model-based approach to estimating circulation from strain consists of an intermediate step of estimating the deformed wing surface is intuitively appealing. It also suggests more accurate approaches to this problem, including relaxing the assumption that all pressure is in a direction purely normal to the undeformed membrane plane.

Results and Discussion

Aerodynamic Loads

In order to verify lift predictions from sensed strain and CFD analysis, each wing configuration was run through aerodynamic load tests. The model was swept through angles of attack from 0 to 20 degrees at an air speed of 18 m/s corresponding to a chord line Re of 90000. Four wing configurations were tested; one with a 0.75mm thick Aluminum plate attached to the wing frame, and three with 0.13mm thick latex membrane stretched over the frame, each with a different level of pre-strain. Membranes with an average percent pre-strain and one standard deviation of 2.13±0.24, 3.36±0.25 and 5.07±0.41 were tested. Values of coefficient of lift versus AOA can be seen in Figure 13 for each lifting surface. Classical behavior is seen in the way the membrane wings continue to increase lift at higher angles of attack where the rigid plate experiences flow separation on the suction surface. It can also be seen that with increased membrane pretension the lift approaches that of the rigid wing.

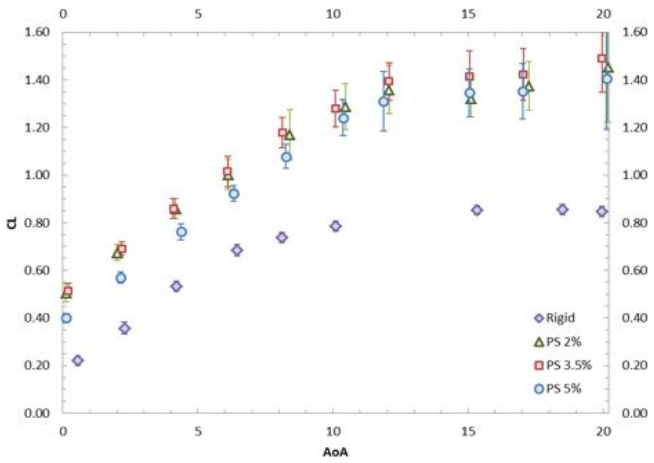

Figure 13. Speckled latex membrane wing during wind tunnel testing (left) and CAD model generated from the strain sensor surface reconstruction.

Surface Reconstruction

For the three different membranes pretensions of 2, 3.5 and 5 percent pre-strain, VIC images were taken at 3, 6 and 9 degrees AOA and each at 12, 15 and 18 meters per second. One sample data set for a 2% pre-strain wing at 6 degrees AOA and 18 m/s can be seen in the left side of Figure 8. Using this data strain sensors were created with quantity, size and positions as defined in Table 2 and as can be seen in Figure 14.

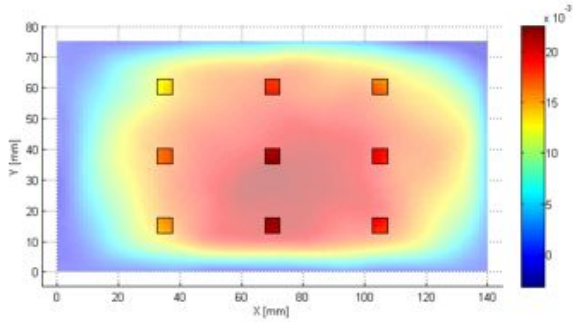

Figure 14. Representation of nine evenly spaced and equally sized strain sensors derived from full field VIC total strain $\left(\varepsilon_x + \varepsilon_y\right)/2$.

Using the methods defined above, the information provided from the stain sensors was used to reconstruct a quadratic representation of actual deformed membrane surface. The reconstructed membrane surface and the location of strain sensors can be seen in the right side of Figure 8 for the 2% pre-strain wing at 6 degrees AOA and 18 m/s.

Table 2. Strain sensor configuration

Sensor	w [mm]	h [mm]	2x/b	y/c
1	5	5	0.5	0.5
2			0.5	0.2
3			0.5	0.8
4			0.25	0.5
5			0.25	0.2
6			0.25	0.8
7			0.75	0.5
8			0.75	0.2
9			0.75	0.8

Comparing the normalized camber, z/c, where z= α*1mm (from Eq. 1.9) and c being the wing chord length in millimeters; for a single membrane at different AOA and wind velocities, we can see from Figure15 a favorable result from the reconstructed surface compared to the actual membrane. The result matches quite well at low AOA and begins to deviate at higher AOA, again as would be expected with such a low order approximation. We can also see an expected increase of camber with respect to velocity and with respect to AOA. Full field error can be seen from the residuals of the reconstructed surface compared to the actual membrane surface from Figure 16. These results are also favorable and show <10% error of max residual compared to maximum deflection, i.e. camber.

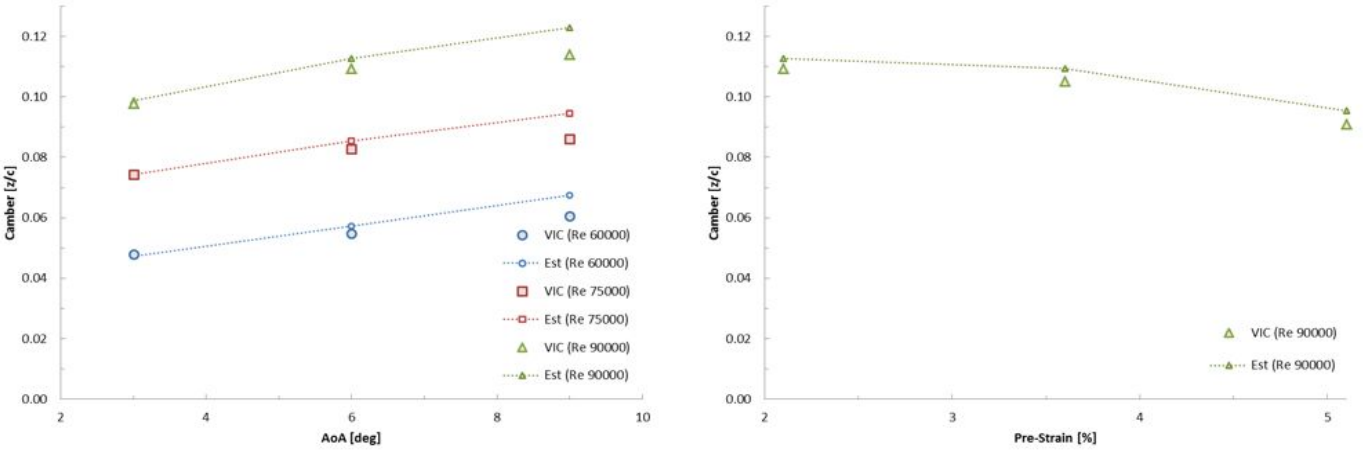

Figure 15. Comparison of normalized camber [z/c] versus AOA, between VIC data (VIC) and strain sensor reconstruction (Est) for a 2% pre-strain membrane at different Re (left), and a comparison of normalized camber versus amount of pre-strain, between VIC data (VIC) and strain sensor reconstruction (Est) for a wing at 6 degrees AOA.

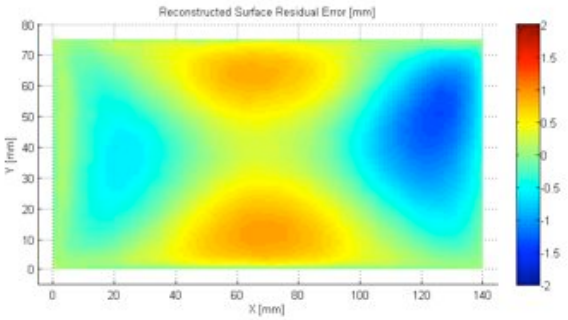

Figure 16. Residual error from out-of-plane deformation of VIC data and reconstructed surface.

Material Characterization

To derive the tension fields in the membrane, the elastic modulus of the latex material was determined empirically. A 25mm by 100mm speckled sample of latex was vertically suspended in front of the same aforementioned cameras used to image the membrane while in the wind tunnel. In this test, weights were applied to one end of the latex and images were taken for each weight. Strains were determined for each load as can be seen in on the left of Figure 17. Due to the hyper elastic behavior of latex, the modulus is not constant throughout deformation. For this reason a quasi linear region is considered between the values of lowest pre-strain and max expected induced strain from loading. For this test strains between 0.02 and 0.10 were observed, thus the modulus of elasticity was assumed to be linear in this region and yielded a magnitude of 1.14 MPa. Since VIC data also provides lateral strain as well as longitudinal strains, the Poisson ratio could be readily determined and was found to be 0.39, results can be seen on the right of Figure 17.

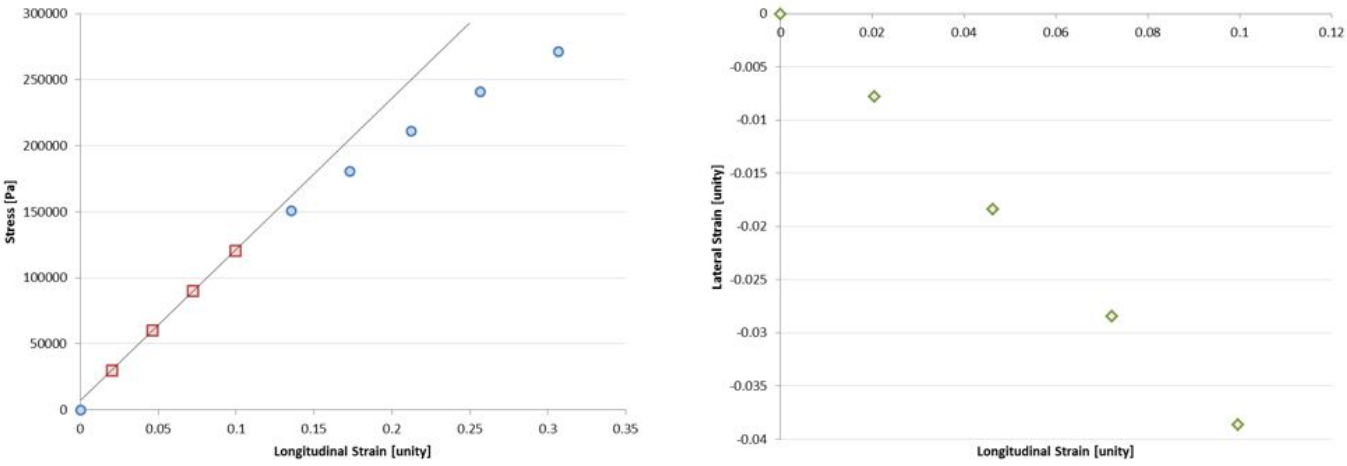

Figure 17. Residual error from out-of-plane deformation of VIC data and reconstructed surface.

Lift Calculation

Using the data collected and methods described above, lift estimations were calculated for the membrane wings using the pseudo strain sensor configuration discussed above. Load estimates as compared to actual load readings from the sting during wind tunnel testing can be seen in Figure 18. As can be easily observed, all loads estimates/calculations are less in magnitude than actual values, which is to be expected due to the low order nature of the methods employed. Comparing the force resultant from the CFD model to measured data, where the CFD value is derived from the integration of the numerical pressure gradient over the entire messed wing surface, yields a result with a constant offset error of ~15%. This constant offset is to be expected from a relatively low fidelity numeric model, but provides confidence that the majority of the wake flow energy will be present in the simulation.

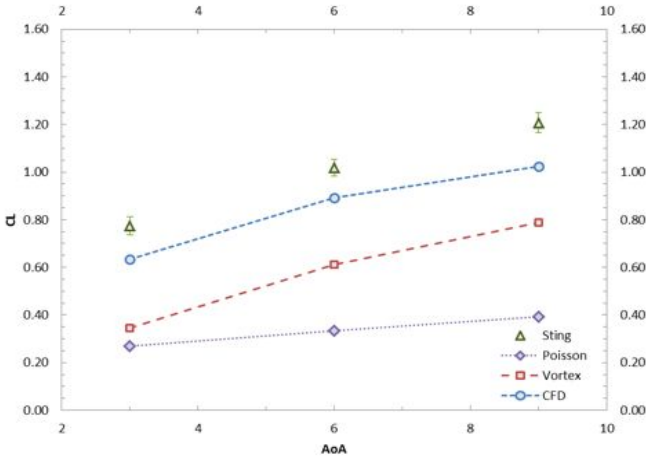

Figure 18. Comparison of aerodynamic load generated at different AOA for a 2% pre-strained wing using various force measuring/estimating techniques; sting balance measurement from wind tunnel tests, force calculation from CFD, force estimation from tip vorticity, and force estimation from Poisson model.

The lift estimation from vorticity showed that the force estimation increases with the same slope as that of the actual lift but is again off by a constant offset of ~50%. This can be attributed to many factors, i.e. theoretical model fidelity, numerical model fidelity, but is likely most significantly affected by the fact that the tip vortex does not contain the complete lift circulation energy and will therefore never be completely capable of providing the full force estimation. Nevertheless, this behavior is certainly correlatable to tangible lift values, derived from strain and vorticity, through the inclusion of a constant offset applied to the result.

Finally, we observe the behavior of the force estimation from the Poisson model. Here we can see estimation behaves very differently from the previous estimation. In this case the model has a constant error of approximately 66%. This allows us to conclude that the force estimation is off by a constant multiple as opposed to the constant offset seen by the vorticity estimation. This again gives rise to a correlatable lift estimation through the inclusion of a constant multiple applied to the result. It is important to note that this estimation has been developed with a low order approximation of the structural form the wing can take and of the dynamic pressure applied to it. With higher order models it is likely that the absolute accuracy of these estimations could be improved. Nevertheless, even with very simple, low order approximations, a distinct correlation between strain, vorticity and lift has been made; within the bounds of this study.

Future Work

This work has strongly encouraged future research in a variety of ways. First, the assumptions that were used in formulating the overall estimation problem were fairly extensive. This was the goal of the present work, however, but nonetheless encourages future research that relaxes the assumptions made including using a single quadratic function for the deformed membrane surface, when it is known that only an infinite Fourier series solution can actually describe such a surface. Relaxing this restriction by truncating the relevant Fourier series solution, arrived at by assuming a specific functional form of F, rather than W, would likely yield better results at the cost of requiring a more complicated least-squares or nonlinear least squares solution, due to the quadratic nature of the strain model.

The classical linear aerodynamic theory that was utilized in this work is also well-known to be problematic at both the scale of MAVs and, in general, is much less accurate that thin airfoil theory, or the suite of panel or vortex lattice codes available. Restricting the approach to be real-time is the main issue facing the choice of aerodynamic approaches and solvers. An investigation of the trade-off of more complex flow and pressure state solver options versus simple aerodynamic principles should also be investigated in the future. Perhaps coupling of a panel solver to a finite element membrane model with strain estimation could yield an algorithm which uses both aerodynamic and structural theory to minimize the estimate error of both load and structural deformation in an iterative fashion.

Finally, as was hypothesized earlier, the main culprit for error is suspected to be the linear membrane model used. This is likely primarily due to the relatively low pretensions used in this work. Validity of membrane models is well documented, and linear membrane models have been demonstrated to provide fair accuracy, even for large deformations, provided pretension is sufficient. However, an obvious tradeoff results from additional pretension as the airfoil behaves more like a thin-plate rather than a highly cambered wing, and thus at some point will experience a loss of lift and efficiency. As before, a balance will likely be achieved by investigating this problem a wider range of pretension and flight regimes.

Acknowledgments

The authors would like to thank the support of the Air Force Office of Scientific Research, Flow Control & Aeroelasticity under Contract FA9550-10-1-0325, with Douglas R. Smith as project monitor and i the Air Force Office of Scientific Research under the Multidisciplinary University Research Initiative grant FA9550-07-1-0540. The authors would also like to acknowledge Dr. Belinda Batten continuous and critical support to the project and the University of Florida for assistance with contractual aspects.

References

1. Shyy, W. (2008) . *Aerodynamics of low Reynolds number flyers*. Cambridge University Press.

2. Sutton, M.A., Cheng, M., Peters, W.H., Chao, Y.J., McNeill, S.R. (1986). Application of an Optimized Digital Correlation Method to Planar Deformation Analysis. *Image and Vision Computing*, 4(3), pp. 143-151.

3. Sutton, M.A., Turner, J. L., Bruck, H. A., Chae, T. A., (1991). Full Field Representation of the Discretely Sampled Surface Deformations for Displacement and Strain Analysis. *Exp. Mech.* 31(2), 168-77.

4. Schmit, R. & Glauser, M. (2005). Use of low-dimensional methods for wake flowfield estimation from dynamic strain. *American Institute of Aeronautics and Astronautics Journal*, 43(5), 1133-1136.

5. Schmit, R. (2002). *Low dimensional tools for flow-structure interaction problems: application to micro air vehicles* (Doctoral dissertation).

6. Song, A., Tian, X. Israeli, E., Galvao, R., Bishop, K. Swartz, S., & Breuer, K. (2008). Aeromechanics of membrane wings with Implications for animal flight. *American Institute of Aeronautics and Astronautics Journal*, 46(8), 2096-2106.

7. Posada, J. A. (2007). *Numerical study of wingtip shed vorticity reduction by wing boundary layer control* (Doctoral dissertation). Available from ProQuest Disserations & Teses database. (Publication no. 3298564)

8. Imamura, T. Enomoto, S. & Yamamoto, K. (2006) Noise Generation Around NACA0012 Wingtip Using Large-Eddy Simulation. *International Congress of the Aeronautical Sciences*, 25, 1-10.

APPENDIX A1

Table 3. Complete Test Matrix

				Quadratic Basis Function W= A*x(x-c/2)*y(y-b)				
				Sensor Configuration 1				
Wind Tunnel Test Matrix				Alpha				
Data Set	PS [%]	AoA	V [m/s]	A_VIC	A_lsq	A_sensor	C_VIC	C_sensor
25	2	3	12	4.02	4.06	3.96	0.05	0.05
			15	6.24	6.31	6.24	0.07	0.07
			18	8.21	8.30	8.29	0.10	0.10
26		6	12	4.60	4.78	4.81	0.05	0.06
			15	6.95	7.14	7.17	0.08	0.09
			18	9.19	9.42	9.46	0.11	0.11
27		9	12	5.09	5.37	5.67	0.06	0.07
			15	7.24	7.61	7.94	0.09	0.09
			18	9.58	10.01	10.32	0.11	0.12
32	3.5	3	12					
			15					
			18					
33		6	12					
			15					
			18	8.84	8.96	9.20	0.11	0.11
34		9	12					
			15					
			18					
18	5	3	12					
			15					
			18					
19		6	12					
			15					
			18	7.64	7.71	8.01	0.09	0.10
20		9	12					
			15					
			18					

Table 4. Complete Test Matrix (continued)

Measured Data From Wind Tunnel Test										
Act V [m/s]	Act AoA [deg]	Act PS_xx [%]	Std PS_xx [%]	Act PS_yy [%]	Std PS_yy [%]	Test PS [%]	Wind Tunnel Loads [N]			
							Sting L	Stg L/2	Sting NF	Stg NF/2
12.1	3.02	2.04	0.21	2.22	0.27	2.13	1.35	0.67	1.35	0.67
15.0	3.04						2.38	1.19	2.39	1.19
18.2	3.07						3.87	1.93	3.89	1.94
12.0	6.14						1.90	0.95	1.90	0.95
15.1	6.16						3.29	1.65	3.31	1.65
18.0	6.19						5.09	2.54	5.14	2.57
12.0	9.09						2.31	1.16	2.34	1.17
14.9	9.12						3.85	1.92	3.90	1.95
18.0	9.16						6.03	3.02	6.14	3.07
12.1	3.06	3.29	0.16	3.43	0.34	3.36	1.38	0.69	1.38	0.69
15.1	3.08						2.47	1.23	2.48	1.24
18.0	3.11						3.84	1.92	3.86	1.93
12.0	6.07						1.95	0.98	1.96	0.98
14.9	6.10						3.32	1.66	3.34	1.67
18.0	6.13						5.20	2.60	5.25	2.62
12.1	9.08						2.42	1.21	2.44	1.22
15.0	9.12						4.00	2.00	4.05	2.03
18.1	9.16						6.16	3.08	6.27	3.14
12.1	3.01	5.03	0.38	5.10	0.44	5.07	1.14	0.57	1.14	0.57
15.1	3.03						2.06	1.03	2.06	1.03
18.0	3.06						3.40	1.70	3.41	1.71
12.1	6.06						1.75	0.87	1.76	0.88
15.1	6.08						3.04	1.52	3.05	1.53
18.1	6.11						4.83	2.42	4.87	2.43
12.0	9.15						2.24	1.12	2.26	1.13
15.0	9.18						3.72	1.86	3.76	1.88
18.0	9.22						5.71	2.85	5.79	2.90

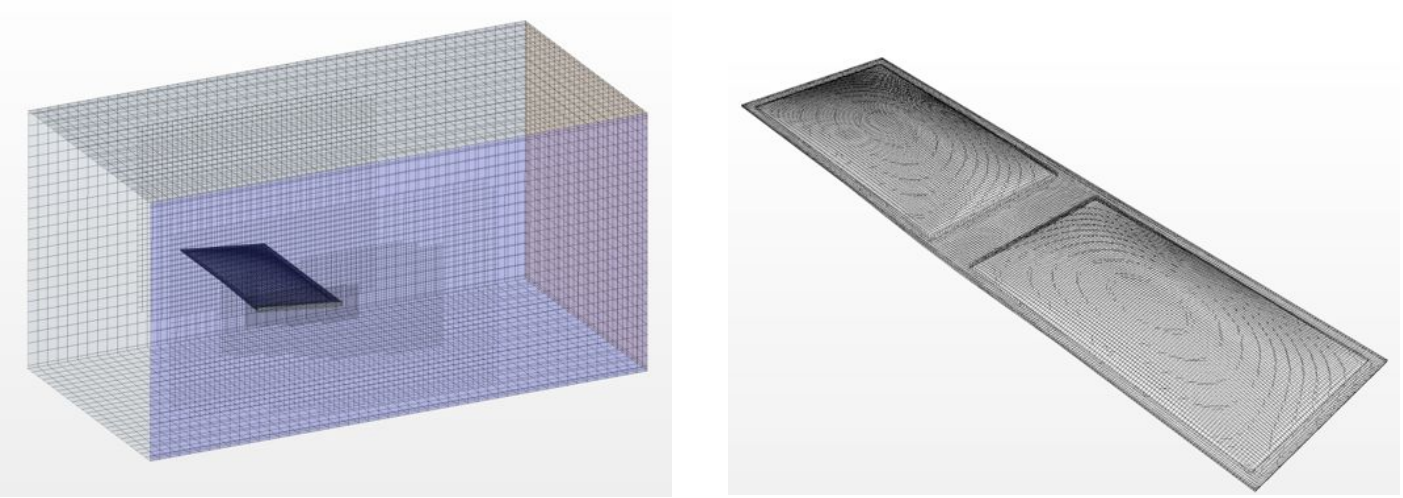

Figure A1-12. Half span CFD simulation domain (left) and meshed membrane wing (right) shown in full span.

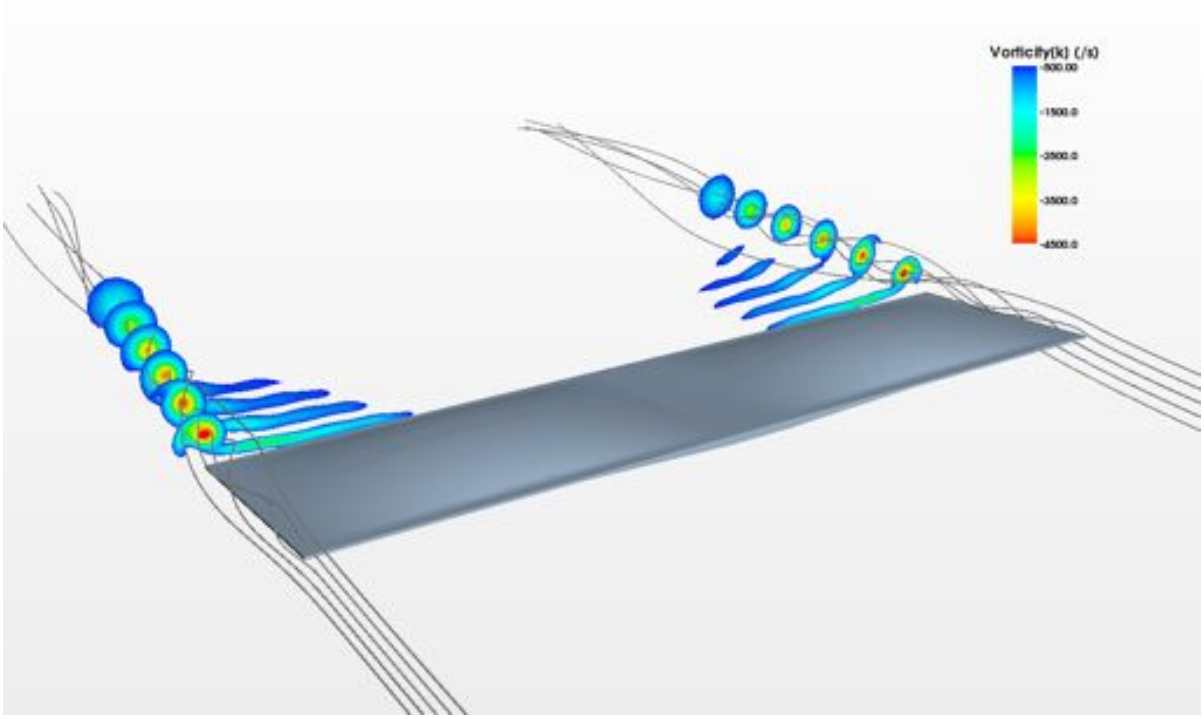

Figure A1-13. Vorticity contours of a 2% pre-strained membrane wing at AOA of 6 degrees and 18m/s.

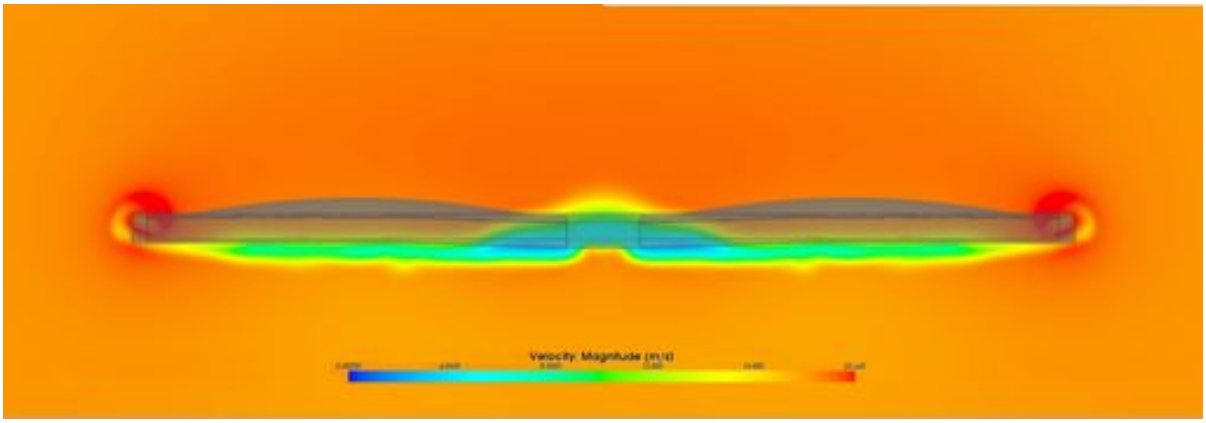

Figure A1-14. Velocity wake contour in m/s, 15mm behind a 2% pre-strained membrane wing at AOA of 6 degrees and 18m/s.

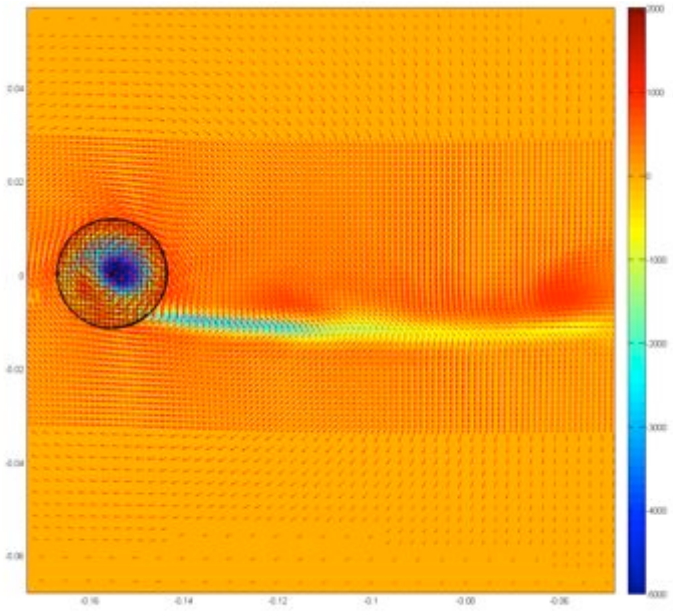

Figure A1-15. Color map showing vorticity contour 15mm behind wing; velocity vector field normal to free stream shown in red vectors; and circulation integration domain of wing tip vortex shown in black.